applied sciences

MDPI

Article

Experimental Study on Axial Stress and Hammer Impacting Energy of Offshore Standard Penetration Test

Miaojun Sun [1], Qianlong Zhang [2], Honglei Sun [2] and Zhenqi Weng [2,*]

[1] Powerchina Huadong Engineering Corporation, Hangzhou 311122, China; sun_mj2@hdec.com
[2] College of Civil Engineering, Zhejiang University of Technology, Hangzhou 310014, China; 18967109940@163.com (Q.Z.); sunhonglei@zju.edu.cn (H.S.)
* Correspondence: 1111802026@zjut.edu.cn

Abstract: Standard penetration test (SPT) has been widely used in offshore exploration because of its unique advantages. Unlike onshore exploration, offshore construction areas are characterized by high waves and water depths ranging from several meters to tens of meters. As a result, the reliability of offshore SPT is significantly reduced compared with onshore SPT. Currently, the probe rod length correction of SPT is not involved in geotechnical engineering investigation codes and related research, which greatly limits the application of this method in offshore exploration. Therefore, a series of SPTs were carried out in offshore environments with different water depths, with a maximum rod length of 65 m. The acceleration and axial stress at each test point of the rod were monitored by the dynamic signal data acquisition system, and the hammer impacting energy at each test point was obtained by Force–Velocity (F-V) method. The test results show that the correction of the rod length of the offshore SPT is different from that of the traditional SPT, and it needs to be further corrected for the water depth. In this paper, a modified method of rod length for offshore SPT is proposed, which can provide reference for the application of offshore SPT.

Keywords: offshore standard penetration test; axial stress; energy efficiency; modified coefficient of rod length

Citation: Sun, M.; Zhang, Q.; Sun, H.; Weng, Z. Experimental Study on Axial Stress and Hammer Impacting Energy of Offshore Standard Penetration Test. *Appl. Sci.* **2023**, *13*, 9487. https://doi.org/10.3390/app13179487

Academic Editor: José António Correia

Received: 12 June 2023
Revised: 26 July 2023
Accepted: 15 August 2023
Published: 22 August 2023

1. Introduction

In recent years, with the rapid development of offshore engineering, it is significant to understand the mechanical engineering properties of seabed soil. Submarine sediments are characterized by loose structure, high water content, and high sensitivity, which make drilling and sampling difficult, and their engineering properties mainly rely on in situ field tests [1].

Standard penetration test (SPT) is a common in situ testing technique with the advantages of simple equipment and wide application. The engineering and mechanical properties of cohesive and sandy soils can be determined by analyzing the blow counts of SPT (N) [2–5]. However, the SPT equipment is not a precision instrument, and the measured N is affected by various factors such as human operation errors and equipment differences. Therefore, it is usually solved by stereotyping equipment specifications, standardizing operation methods, and limiting the scope of application.

For SPT in shallow marine soft soils, since the survey hole is deep (generally tens of meters), the blow counts are affected by the rod length; therefore, the length correction must be carried out. Some suggestions have been given in domestic and foreign related norms and studies on the rod length correction of the measured penetration blow counts in the analysis of the results of the SPT [6–11]. In addition, many scholars have also studied SPT from the hammer impacting energy for an accurate evaluation of the N value [12–24]. According to the theory of one-dimensional rod stress wave propagation, Zuo et al. [25] obtained the correction coefficient for the rod length within the range of 36 m through the

indoor model test. In addition, Zuo et al. [26] obtained the rod length correction coefficient in the range of 83 m by indoor model tests and found that the rod length correction coefficient was independent of the foundation soil material properties by comparison tests of soils with different properties. Shi et al. [27] studied the axial stress and hammer impacting energy distribution along the probe rod based on the field dynamic penetration test and established the relationship equation between hammer impacting energy and rod length. Using experimental and numerical simulation methods, Li et al. [28] analyzed the hammer impacting energy distribution in the probe rod and gave the rod length correction coefficient in the range of 72 m rod length. However, the existing studies mainly focus on onshore dynamic penetration test, while the influence of the deflection and deformation of the probe rod and the shaking of the ship-mounted drilling platform on the rod length correction coefficient in the offshore environment is not considered [29].

In this study, a series of on-site in situ tests was carried out to analyze the axial stress distribution and acceleration changes during the hammering process of the probe rod in the offshore environment. The difference in the transmission efficiency of hammer impacting energy of probe rods with different lengths is further revealed, and a rod length correction method suitable for the offshore SPT is proposed, which provides a reference for the offshore SPT.

2. Offshore SPT

2.1. Test Site

This test is based on the offshore wind farm project of China Guangdong Nuclear Corporation Limited, and the test site is located in the northeastern sea area of Xiangshan County, Zhejiang Province. The distance from the site center to the shore is 8.2 km, and the depth of seawater in the site is 5.0–25.2 m. The seabed geological profile of the test site is shown in Figure 1, and the soil properties for different layers are presented in Table 1. The SPT is carried out on the survey test platform.

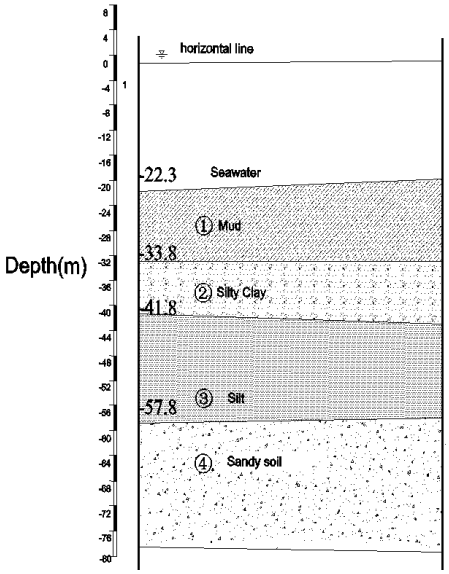

Figure 1. Geological profile of the test sea area.

Table 1. Index properties of soils at the site located in the northeastern sea area of Xiangshan 71 County, Zhejiang Province.

Soil Layers	Properties								
	Water Content/ %	Density/(g/m^3)	Specific Density	Void Ratio	Liquid Limit/%	Plastic Limit/%	Compression Modulus/ MPa	Cohesion Force/kPa	Internal Friction Angle/°
Mud (−22.3 m~−33.8 m)	57.2	1.65	2.74	1.60	46.2	27.2	2.39	11.0	8.3
Silty clay (−33.8 m~−41.8 m)	24.8	2.02	2.73	0.69	39.7	23.9	6.90	52.0	16.2
Silty (−41.8 m~−57.8 m)	27.2	1.96	2.70	0.75	/	/	7.66	8	31.6
Sandy soil (−57.8 m~)	21.1	1.99	2.69	0.63	/	/	8.97	3	33.9

2.2. Test Scheme

In terms of the probe rod used in the field SPT, the outer diameter is 50 mm, the inner diameter is 31 mm, the density is 7.85×10^3 kg/m^3, and the elastic modulus is 2.11×10^{11} Pa. A total of three strain and acceleration test points are arranged along the rod, which are, respectively, 0.5 m away from the anvil at the top of the rod, at the water–soil contact surface, and 0.5 m above the rod bottom penetrator, as shown in Figure 2. The strain of the probe rod is measured by 120-3AA-type strain gauges. Each measuring point is arranged with four strain gauges at right angles and connected by the full bridge method. The acceleration of the probe rod is measured by the acceleration sensor, and its maximum range is 4.5×10^4 m/s^2, which meets the test requirements. The strain and acceleration data are collected by the DH5922D dynamic signal data collection system, which includes eight data collection channels. The maximum continuous sampling rate is 200 kHz, which can meet the requirements of dynamic strain and acceleration data collection in the test.

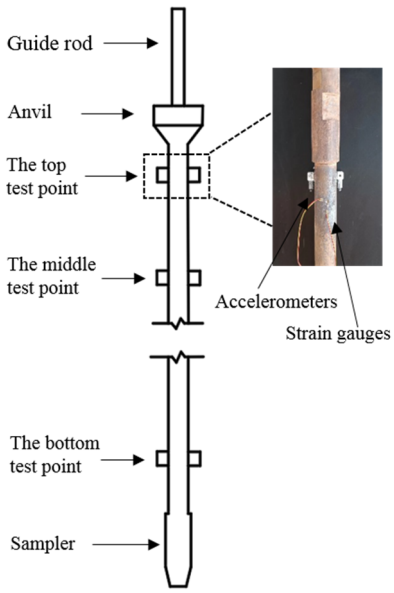

Figure 2. Layout of probe rod test points.

During the test, the weight of the drop hammer is 63.5 kg and the lifting height is 76 mm. An automatic hoist is used to control the hammering rate and lifting height. In the test, the blow rate is about 20 strokes per minute, which meets the requirements of the specification. In order to ensure the accuracy of the test results, parallel tests were carried out in different test groups.

There are eight test points in the test site for SPT. Before the test, the water depth of the site was initially surveyed. The water depths of the eight test points were 7.1, 8.9,

11.1, 11.6, 15.0, 17.1, 19.4, and 20.7 m, respectively. For each test site, 10 sets of standard penetration tests were designed for different rod lengths to investigate the hammering energy transmission efficiency of the probe rod at survey depths of 5, 10, 15, 20, 25, 30, 35, 40, 45, and 50 m, respectively.

3. Results

3.1. Stress Wave Propagation Velocity Analysis

From the one-dimensional wave theory, the theoretical wave velocity in the probe rod can be calculated from Equation (1) [30–36]:

$$C = \sqrt{E/\rho} \quad (1)$$

where C is the wave velocity (m/s), E is the static elastic modulus of the probe rod (10^9 Pa, the average elastic modulus of the probe rod in the test is 195×10^9 Pa), and ρ is the probe rod density (value is 7850 kg/m^3). The theoretical wave velocity in the probe rod is 4987.5 m/s.

Wave velocity between test points in the probe rod is equal to the spacing between test points divided by the time interval between axial stress peaks at the test points. The measured wave velocities between the test points are presented in Table 2. Comparing the measured data in Table 2, it can be seen that the measured wave velocity of the probe rod is 4547.7~4752.6 m/s and the measured wave velocity is less than the theoretical wave velocity, which is about 91.2–95.3% of the theoretical value. The theoretical wave velocity is derived from an ideal one-dimensional elastic isotropic rod. Considering that the probe rods are connected in the form of joints, joint looseness, sediment infiltration, and other factors will affect the measured wave velocity, so the measured wave velocity deviates from the theoretical wave velocity and it can be considered that the test results are consistent with the one-dimensional wave theory.

Table 2. Times of peak axial stress for test points.

Distances between Two Test Point/m	Time Intervals between Two Test Point/s	Stress Wave Velocities /m
18.6	0.004090	4547.7
18.6	0.004052	4590.3
18.6	0.004058	4583.5
28.6	0.006056	4722.6
28.6	0.006121	4672.4
28.6	0.006135	4661.8
38.6	0.008124	4751.4
38.6	0.008198	4708.5
38.6	0.008173	4722.9
48.6	0.010226	4752.6
48.6	0.010273	4730.8
48.6	0.010366	4688.4

3.2. Probe Rod Axial Stress and Acceleration Analysis

Figure 3 shows the axial stress change with time at the top of the probe rod and at the water–soil contact surface under different water depths. In this representation, negative stress indicates the probe rod being subjected to compression, while positive stress indicates tension on the probe rod. It can be clearly observed that there are multiple stress peak points, which are caused by secondary hammering due to rebound after the anvil is struck by the falling hammer. In this paper, only the axial stresses and acceleration changes of the rod produced by the first hammering are analyzed. As can be seen from Figure 3, the stress wave formed by the impact of the falling hammer on the probe rod gradually decays in the process of downward propagation, resulting in a significant reduction in the peak axial stress from the top to the bottom of the rod. With the increase in the test water depth, there

is no significant difference in the peak axial stress at the top test point, but the peak stress at the bottom test point decreases with the increase in water depth. Compared with the test group with a test water depth of 7.1 m, the peak stress at the top test point in the test group with a test water depth of 17.1 m decreased by 2.1%, while the peak stress at the bottom test point decreased by 28.2%.

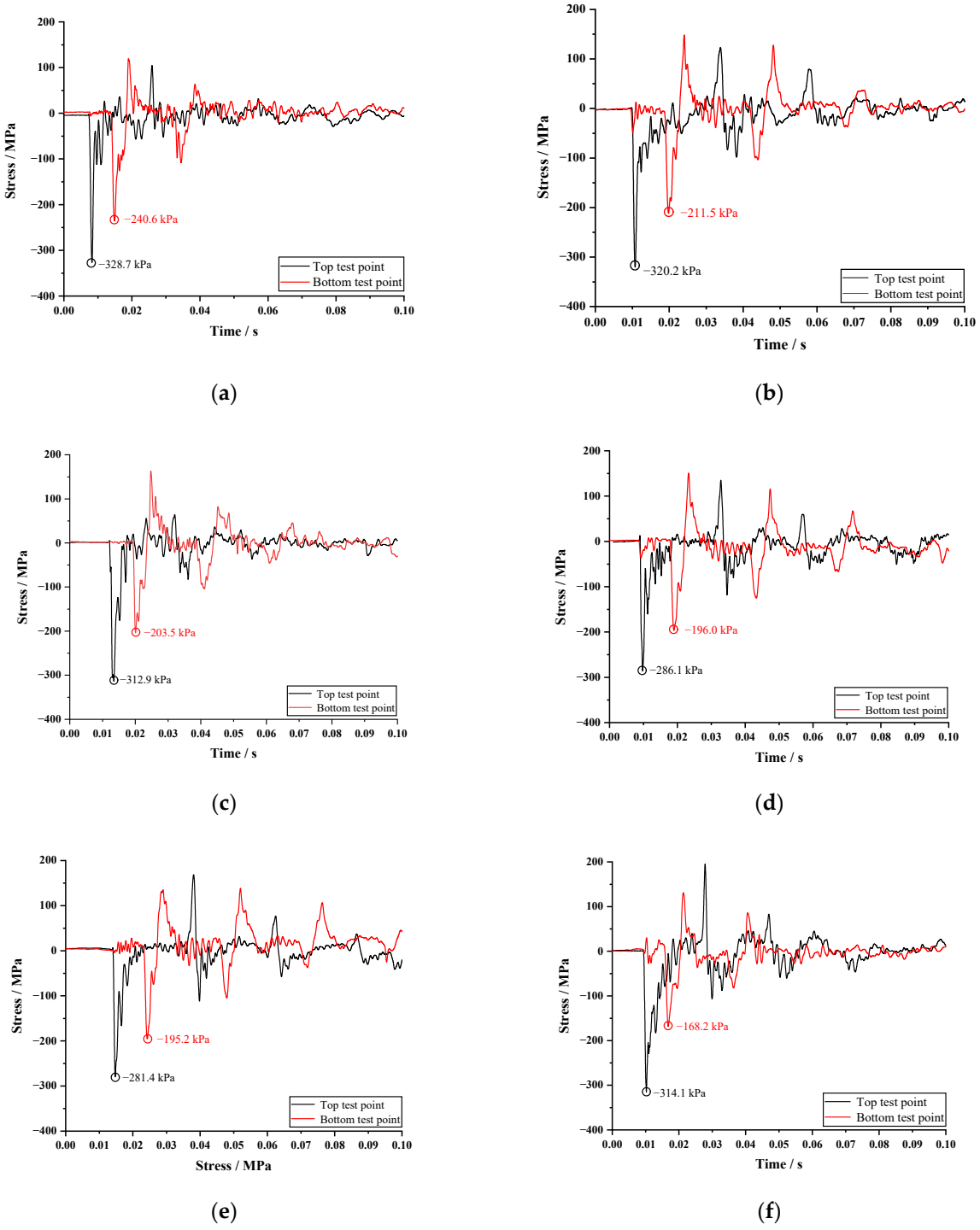

Figure 3. *Cont.*

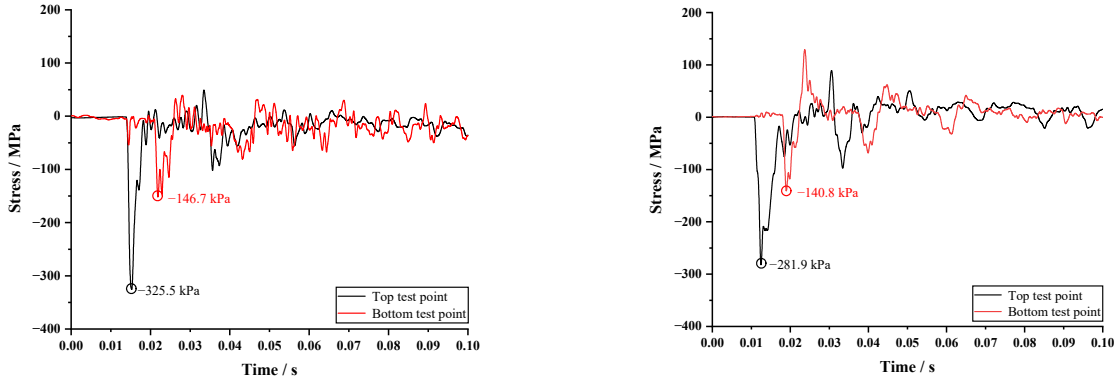

(**g**) (**h**)

Figure 3. Relationship between axial stress of probe rod and time under different water depths. (**a**) Water depth of 7.1 m; (**b**) water depth of 8.9 m; (**c**) water depth of 11.1 m; (**d**) water depth of 11.6 m; (**e**) water depth of 15.0 m; (**f**) water depth of 17.1 m; (**g**) water depth of 19.4 m; (**h**) water depth of 20.7 m.

Figure 4 shows the effect of survey depth on the axial stress at the top and bottom test points of the probe rod under a water depth of 15 m. As can be seen from Figure 4, there is a significant difference in the magnitude of peak stress between the top and bottom test points of the probe rod. The axial stress at the bottom test point is notably smaller than that at the top test point. For example, at a survey depth of 10 m, the peak stress at the top test point is 308.4 MPa, while the peak stress at the bottom test point is 124.6 MPa, a reduction of 59.6%. With the increase in the length of the probe rod, there is no significant difference in the peak stress at the top test point, and the peak stress at the bottom test point decreases with the increase in the rod length. Compared with the test group with a survey depth of 10 m, the stress at the top test point was reduced by 4.8% and the stress at the bottom test point was reduced by 11.5% for the test group with a survey depth of 20 m.

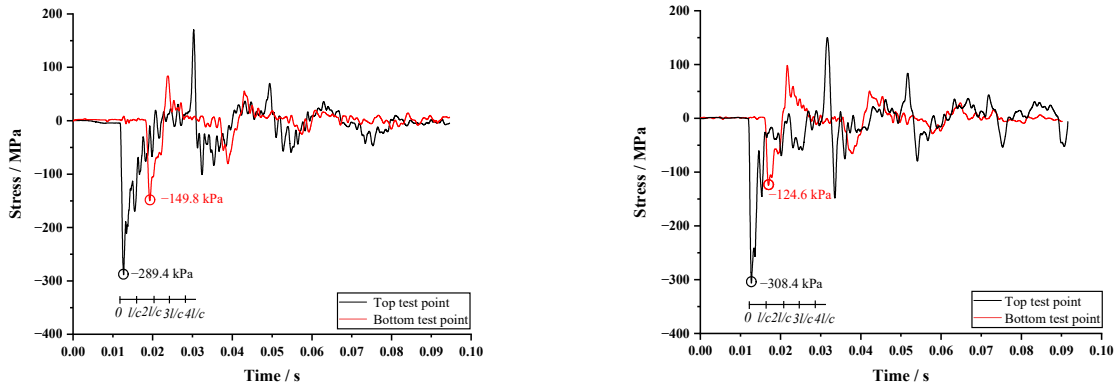

(**a**) (**b**)

Figure 4. *Cont.*

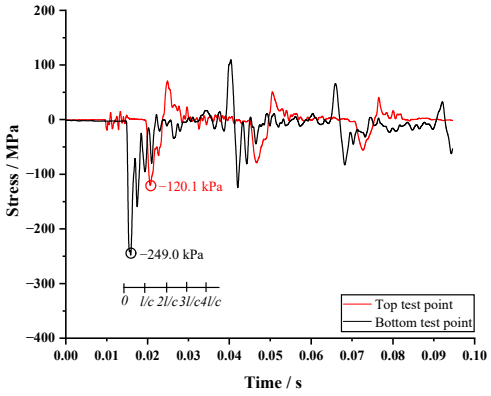

(**c**)

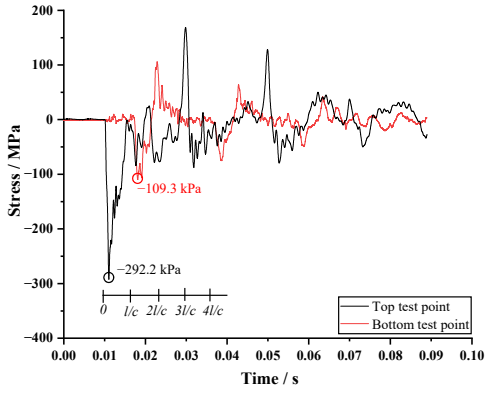

(**d**)

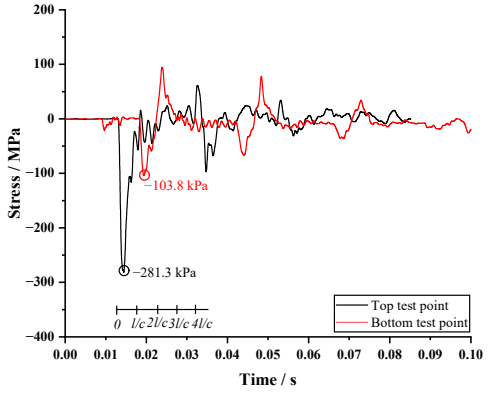

(**e**)

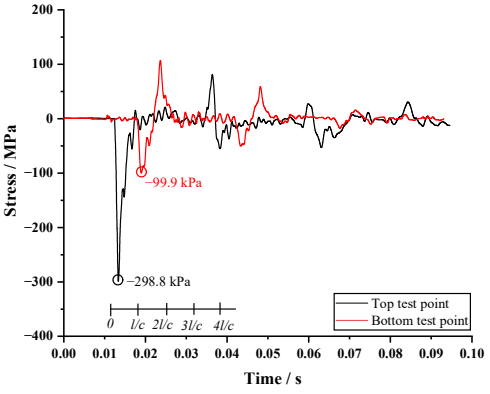

(**f**)

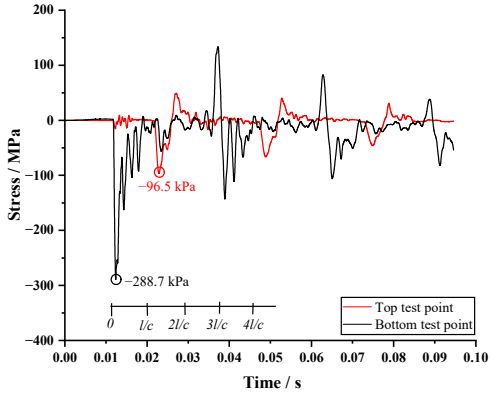

(**g**)

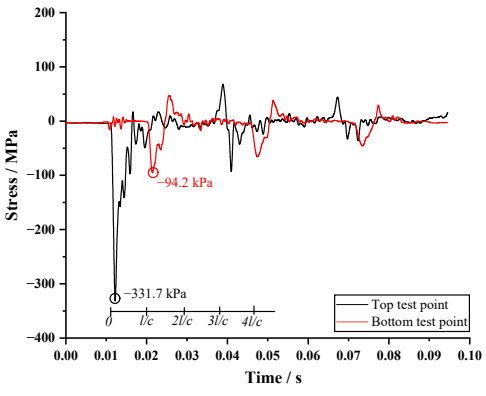

(**h**)

Figure 4. *Cont.*

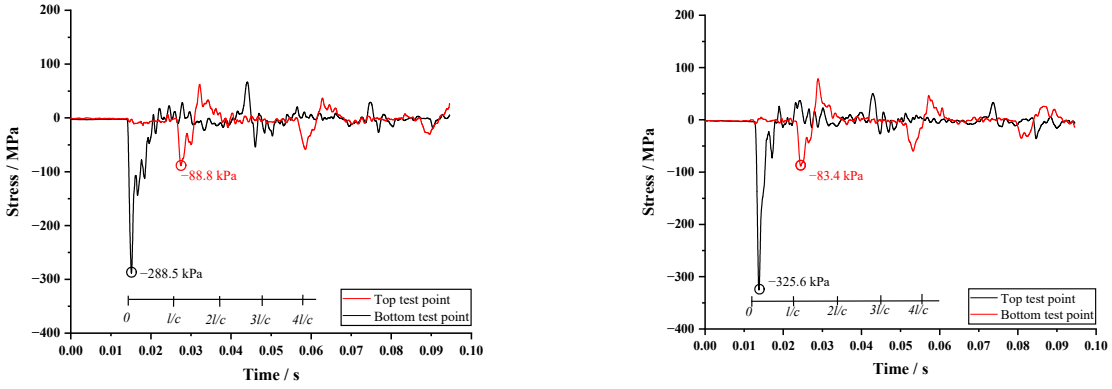

(**i**) (**j**)

Figure 4. Relationship between the axial stress of the probe rod and time. (**a**) Survey depth of 5 m; (**b**) survey depth of 10 m; (**c**) survey depth of 15 m; (**d**) survey depth of 20 m; (**e**) survey depth of 25 m; (**f**) survey depth of 30 m; (**g**) survey depth of 35 m; (**h**) survey depth of 40 m; (**i**) survey depth of 45 m; (**j**) survey depth of 50 m.

Figure 5 shows the variation curve of the probe acceleration with time for different rod lengths. With the increase in rod length, the peak acceleration of the rod decreases obviously. For the test group with survey depth of 5–50 m, the peak accelerations are 4975.8, 4923.2, 4672.1, 4501.7, 4399.1, 4267.5, 4192.3, 4087.2, 3957.8, and 3952.7 m/s^2, respectively.

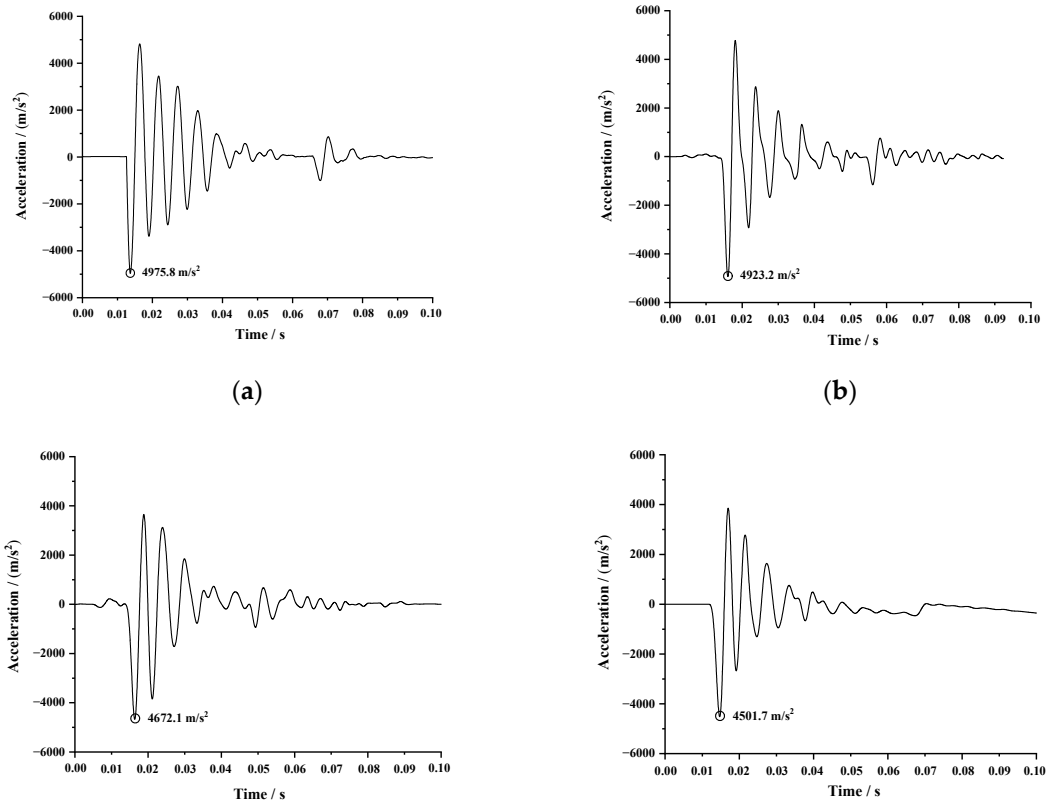

(**a**) (**b**)

(**c**) (**d**)

Figure 5. *Cont.*

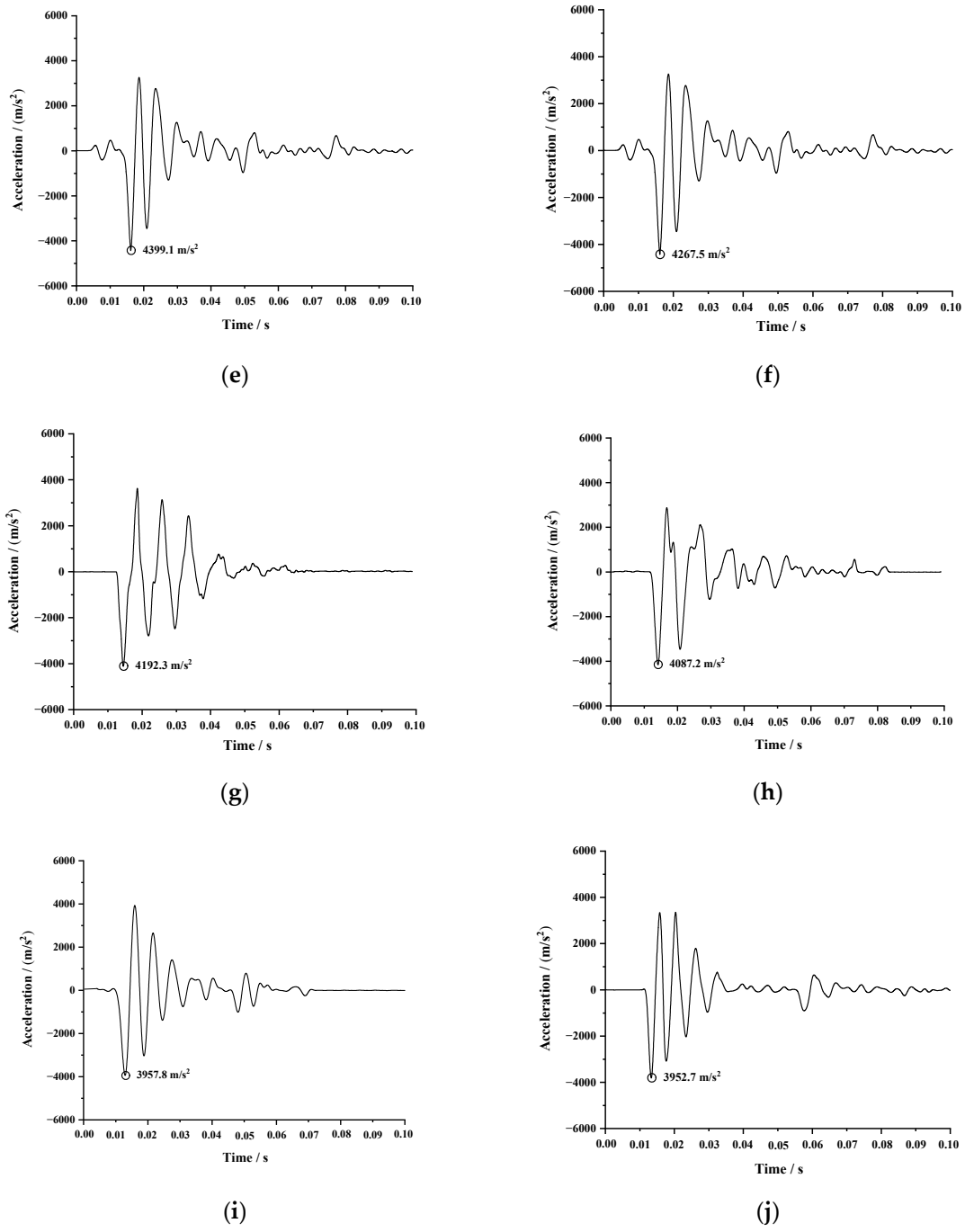

Figure 5. Relationship between probe rod acceleration and time. (**a**) Survey depth of 5 m; (**b**) survey depth of 10 m; (**c**) survey depth of 15 m; (**d**) survey depth of 20 m; (**e**) survey depth of 25 m; (**f**) survey depth of 30 m; (**g**) survey depth of 35 m; (**h**) survey depth of 40 m; (**i**) survey depth of 45 m; (**j**) survey depth of 50 m.

4. Hammer Impacting Energy Transfer Efficiency of Offshore SPT

In our study, force–velocity method (F-V method) is used to calculate the hammer impacting energy distribution in SPT. The F-V method was proposed by Abou-mater and Goble in 1997 [37]. The principle is that the elongated ratio of the rod in the SPT equipment can meet the one-dimensional propagation theory of elastic wave; that is, the transverse propagation of elastic wave is ignored in the process of energy calculation. When the elastic stress wave passes through the position of the dynamometer, the work done by the

stress wave on the point is equal to the product of the force measured at the point and the displacement, and the expression is shown in Equation (2).

$$E_m = \int_0^t F(t)V(t)dt \tag{2}$$

where E_m is the hammer impacting energy obtained by calculation (J), $F(t)$ is axial stress (N), V is the particle velocity of the rod (m/s), and t is the time when the energy accumulates to the maximum energy (s).

4.1. The Effect of Water Depth on the Hammer Impacting Energy Distribution of the Probe Rod

The hammer impacting energy varying with the water depth at the top of the probe rod and water–soil contact surface is shown in Figure 6. The test results show that the water depth has a great influence on the hammer impacting energy distribution in the probe rod. The hammer impacting energy at the top test point increased with the rod length. For the test groups with water depths of 7.1, 8.9, 11.1, 11.9, 15.0, 17.1, 19.4, and 20.7 m, the hammering energies at the top test point are 399.7, 403.1, 408.1, 405.4, 403.2, 405.8, 408.1, and 409.6 J, respectively. The total potential energy of the hammer before falling in the SPT was 473.5 J, so the energy transfer efficiency at the top test point in each test group was 84.4, 85.13, 86.2, 85.6, 85.2, 85.7, 86.2, and 86.5%, respectively. The hammer impacting energy at the test point of water–soil contact surface decreases gradually with the increase in the probe rod length. Compared with those at the top test points, the hammer impacting energies decrease by 19.1, 20.8, 22.5, 22.2, 22.6, 23.3, 24.2, and 24.6%, respectively, and the attenuation value increases with the increase in water depth.

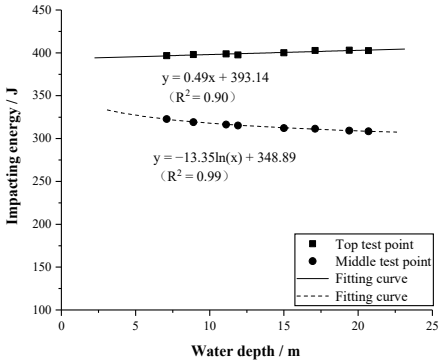

Figure 6. Relationship between hammer impacting energy and water depth of SPT.

By fitting the data in Figure 6, the relationship between the hammer impacting energy and probe rod length at the top of the probe rod and water–soil contact surface can be obtained:

$$E_r = 0.49 \times l + 391.14 \text{ (top test point)} \tag{3}$$

$$E_r = -13.35\ln(l) + 348.89 \text{ (water-soil contact surface)} \tag{4}$$

where l is the water depth (m).

4.2. Effect of Survey Depth on the Hammer Impacting Energy Distribution of the Probe Rod

Figure 7 shows the influence of survey depth on the distribution law of hammer impacting energy under 15 m water depth. Table 2 shows that the hammer impacting energy at the top test points increases with the increase in survey depth. For the test group with a survey depth of 5–50 m, the hammer impacting energies at the top test points are 396.7, 396.2, 392.8, 398.2, 401.2, 406.9, 414.6, 411.3, 412.3, and 414.7 J, respectively, and the energy transfer efficiency at the rod top test points of each test group is 83.8, 83.7, 83.0, 84.1, 84.7, 85.9, 87.6, 86.9, 87.1, and 87.6%, respectively. The hammer impacting energy at the

bottom test points of the probe rod gradually decreases with the increase in the probe rod. The energy transfer efficiency at the top and bottom test points was 81.0, 76.1, 71.9, 66.9, 64.4, 60.5, 57.5, 55.0, 53.8, and 51.6%, respectively.

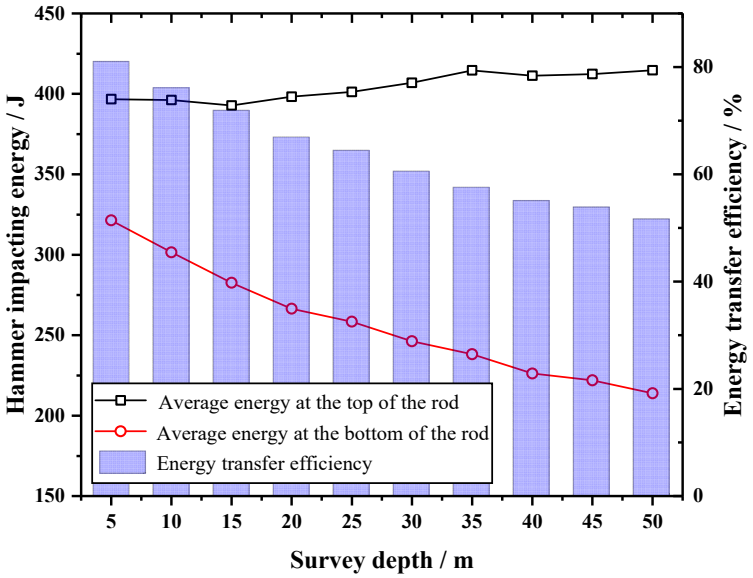

Figure 7. Hammer impacting energy transfer efficiency of SPT.

Figure 8 illustrates the fitting curve for the effective hammering energy of the probe rod with respect to the test depth, as shown in the following equation:

$$E_r = -38.35 \ln(l) + 375.42 \text{ (bottom test point)} \quad (5)$$

where l is the water depth (m).

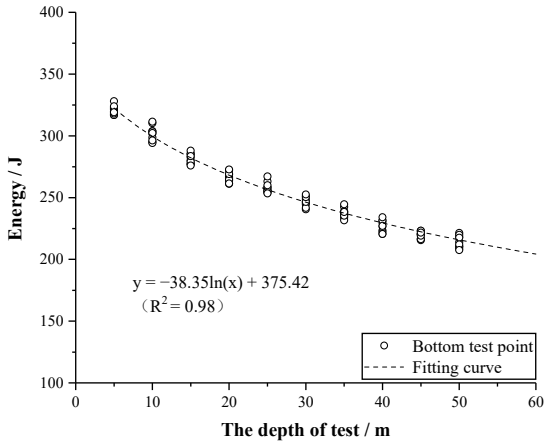

Figure 8. Relationship between hammer impacting energy and test depth.

4.3. Rod Length Correction of Offshore SPT

Effective hammer impacting energy is used to represent the rod length correction in the land SPT (effective hammer impacting energy is the work conducted by the probe penetrating into the soil to overcome the resistance of the soil under the action of one hammering):

$$\alpha = \frac{E_{(l)}}{E_{(2)}} \quad (6)$$

where $E_{(l)}$ is the effective hammer impacting energy of SPT with different rod lengths (J); $E_{(2)}$ is the effective hammer impacting energy of the SPT at the rod length of 2 m (J); and α is the rod length correction coefficient. During the offshore SPT, the influence of the water depth on the hammer impacting energy attenuation in the probe cannot be ignored. Therefore, it is necessary to introduce a water depth correction coefficient to ensure the accuracy of the exploration data. In this paper, the average hammer impacting energy at the top test points under different water depths is used as the correction base point, and the ratio of its hammer impacting energy to that of the probe rod at the water–soil contact surface is defined as the water depth correction coefficient:

$$\alpha_{\mathrm{w}} = \frac{E_1}{E_2} \tag{7}$$

where E_1 is the average value of hammer impacting energy of the probe rod at the water–soil contact surface (J); E_2 is the average value of hammer impacting energy at the top test points (J); and α_{w} is the correction coefficient of water depth. The effect of exploration depth on hammer impacting energy distribution is described, and a survey depth correction coefficient for the offshore SPT is proposed:

$$\alpha_{\mathrm{s}} = \frac{E_l}{E_3} \tag{8}$$

where E_l is the effective hammer impacting energy of SPT with different survey depths (J); E_3 is the effective hammer impacting energy of the SPT at the survey depth of 2 m (J); and α_{s} is the correction coefficient of survey depth. The correction method of blow counts in offshore SPT can be expressed as:

$$N_1 = \alpha_{\mathrm{w}}\alpha_{\mathrm{s}}N \tag{9}$$

where N_1 is the blow counts after correction and N is the measured blow counts in the field.

5. Conclusions

(1) The variation curves of acceleration and axial stress of the probe rod during the hammering process were measured by the offshore SPT. The difference between the measured wave speed and the theoretical wave speed in the test is 4.7–8.8%, which is consistent with the one-dimensional wave theory. The test results show that, as the length of the probe rod grows, the peak acceleration decreases significantly, the peak stress at the top of the rod is basically unchanged, and the peak stress at the bottom of the rod decreases significantly.

(2) The hammer impacting energy at the test points at both ends of the probe rod was obtained using the F-V method based on the one-dimensional wave theory. By analyzing the effective hammer impacting energy distribution of the probe rod under different water depth and survey depth conditions, the relationship between hammer impacting energy and rod length at the top of the rod, water–soil contact surface, and the bottom of the rod is obtained.

(3) According to the definition of rod length correction coefficient and test results, this paper proposes a correction method for blow counts applicable to offshore SPT.

Author Contributions: Conceptualization, M.S.; Methodology, Z.W.; Software, Q.Z.; Investigation, Q.Z.; Resources, M.S.; Data curation, Q.Z.; Writing—original draft, Z.W.; Writing—review & editing, Z.W.; Visualization, H.S.; Project administration, M.S.; Funding acquisition, M.S. and H.S. All authors have read and agreed to the published version of the manuscript.

Funding: "Pioneer" and "Leading Goose" R&D Program of Zhejiang (NO. 2022C03009).

Institutional Review Board Statement: Not applicable.

Informed Consent Statement: Not applicable.

Data Availability Statement: The data that support the findings of this study are available from the corresponding author upon reasonable request.

Conflicts of Interest: The authors declare no conflict of interest.

References

1. Chen, P.X.; Pan, G.F.; Xu, J.L.; Chen, X.L.; Li, D. Correlative study of cone penetration test parameters and physico-mechanical properties of the seabed soil on the East China Sea Continental Shelf. *Geotech. Investig.* **2009**, *37*, 34–37. (In Chinese)
2. Meyerhof, G.G. Penetration test and bearing capacity of cohesionless soils. *Soil Mech. Found. Eng. Engl. Transl.* **1956**, *82*, 1–19. [CrossRef]
3. Robertson, P.K.; Campanella, R.G.; Wightman, A. SPT-CPT correlation. *J. Geotech. Eng. Div.* **1983**, *109*, 1449–1459. [CrossRef]
4. Wang, S.J.; He, M.C.; Zhang, J.Z. Estimation of relative density of sand with normalized standard penetration N value. *Chin. J. Geotech. Eng.* **2005**, *27*, 682–685.
5. Hettiarachchi, H.; Brown, T. Use of SPT Blow Counts to Estimate Shear Strength Properties of Soils: Energy Balance Approach. *J. Geotech. Geoenviron. Eng.* **2009**, *135*, 830–834. [CrossRef]
6. Seed, H.B.; Tokimatsu, K.; Harder, L.F.; Chung, R.M. The influence of SPT procedures in evaluating soil liquefaction resistance. *J. Geotech. Eng. Div.* **1985**, *111*, 1425–1445. [CrossRef]
7. Skempton, A.W. Standard penetration test procedures and the efforts in sands overburden pressure, relative density, particle size, ageing and over-consolidation. *Geotechnique* **1986**, *36*, 425–447. [CrossRef]
8. Daniel, C.; Howie, J.; Jackson, R.; Walker, B. Review of Standard Penetration Test Short Rod Corrections. *J. Geotech. Geoenviron. Eng.* **2005**, *131*, 489–497. [CrossRef]
9. *ISO 22476-2*; Geotechnical Investigation and Testing-Field Testing-Part 2: Dynamic Probing. ISO: Geneva, Switzerland, 2005.
10. *JIS A1219-2001*; Standard Penetration Test Method. Japanese Industrial Standards Committee: Tokyo, Japan, 2001.
11. *ASTM D4633-10*; Standard Test Method for Stress Wave Energy Measurement for Dynamic Penetrometer Testing Systems. American Society for Testing and Materials (ASTM): West Conshohocken, PA, USA, 2010.
12. Kovacs, W.D. Velocity measurement of free-fall SPT hammer. *J. Geotech. Eng. Div.* **1979**, *105*, 1–10. [CrossRef]
13. Rahimi, S.; Wood, C.M. Influence of soil aging on SPT-Vs correlation and seismic site classification. *Eng. Geol.* **2020**, *272*, 105–653. [CrossRef]
14. Schmertmann, J.H.; Palacios, A. Energy Dynamics of SPT. *J. Geotech. Eng. Div.* **1979**, *105*, 909–926. [CrossRef]
15. EI-Sherbiny, R.M.; Salem, M.A. Evaluation of SPT energy for Donut and Safety hammers using CPT measurements in Egypt. *Ain Shams Eng. J.* **2013**, *4*, 701–708. [CrossRef]
16. Yokel, F.Y. Energy transfer in standard penetration test. *J. Geotech. Eng. Div.* **1982**, *108*, 1197–1202. [CrossRef]
17. Matsumoto, T.; Sekiguchi, H.; Yoshida, H.; Kita, K. Significance of two-point strain measurement in SPT. *Soils Found.* **1992**, *32*, 67–82. [CrossRef] [PubMed]
18. Lu, C.H.; Wang, J. Correlations between Vs and SPT-N by different borehole measurement methods: Effect on seismic site classification. *Bull. Earthq. Eng.* **2020**, *18*, 1139–1159. [CrossRef]
19. Tsai, J.S.; Liou, Y.J.; Liu, F.C.; Chen, C.H. Effect of hammer shape on energy transfer measurement in the standard penetration test. *Soils Found.* **2004**, *45*, 103–114. [CrossRef]
20. Odebrecht, E.; Schnaid, F.; Rocha, M.M.; Bernardes, G.P. Energy efficiency for standard penetration tests. *J. Geotech. Geoenviron. Eng.* **2005**, *131*, 1252–1263. [CrossRef]
21. Sancio, R.B.; Bray, J.D. An assessment of the effect of rod length on SPT energy calculations based on measured field data. *Geotech. Test. J.* **2005**, *28*, 22–30.
22. Youd, T.; Bartholomew, H.W.; Steidl, J.H. SPT hammer energy ratio versus drop height. *J. Geotech. Geoenviron. Eng.* **2008**, *134*, 397–400. [CrossRef]
23. Lee, C.; Lee, J.S.; An, S.; Lee, W. Effect of Secondary Impacts on SPT Rod Energy and Sampler Penetration. *J. Geotech. Geoenviron. Eng.* **2010**, *136*, 522–526. [CrossRef]
24. Moghaddam, R.B.; Lawson, W.D.; Jayawickrama, P.W. Hammer Efficiency and Correction Factors for the TxDOT Texas Cone Penetration Test. *Geotech. Geol. Eng.* **2017**, *35*, 2147–2162. [CrossRef]
25. Zuo, Y.Z.; Cheng, Z.L.; Ding, H.S.; Liao, J.H. Study of modified coefficient of dynamic penetration rod length. *Rock Soil Mech.* **2014**, *35*, 1284–1288. (In Chinese)
26. Zuo, Y.Z.; Zhao, N. Model tests on modified coefficient of heavy dynamic penetration rod length. *Chin. J. Geotech. Eng.* **2016**, *38*, 178–183. (In Chinese)
27. Shi, L.; Fu, S.J.; Yuan, W.C.; Han, Y.H.; Zhao, M.J. Experimental study on axial impacting force and hammer impacting energy in rod of heavy dynamic penetration test. *Chin. J. Rock Mech. Eng.* **2016**, *35*, 201–208. (In Chinese)
28. Li, H.Z.; Guo, F.; Fu, S.J.; Hao, W.Z.; Li, Z. Adaptation and correction of dynamic penetration rod length. *Earth Sci.* **2016**, *41*, 1249–1258. (In Chinese)
29. Chai, J.F.; Chen, Z.Y. Influence of drill rod's flexural deflection on standard penetration test in deep bore-holes in maritime spaces. *China Harb. Eng.* **2016**, *36*, 40–43. (In Chinese)

30. Jakeman, D.; Smith, B.L.; Heer, W. *Propagation of Pressure Waves through Airwater Mixtures (No. EIR-534)*; Eidgenoessisches Inst. fuer Reaktorforschung: Lausanne, Switzerland, 1984.
31. Atabek, H.B.; Lew, H.S. Wave propagation through a viscous incompressible fluid contained in an initially stressed elastic tube. *Biophys. J.* **1996**, *6*, 481–503. [CrossRef]
32. Yu ST, J.; Chen, Y.Y.; Yang, L. Velocity-Stress Equations for Wave Propagation in Anisotropic Elastic Media. In *Wave Processes in Classical and New Solids*; IntechOpen: London, UK, 2012.
33. Moradi, S.; Lawton, D.C. Velocity-Stress Finite-Difference Modeling of Poroelastic Wave Propagation. 2013. Available online: https://www.crewes.org/Documents/ResearchReports/2013/CRR201361.pdf (accessed on 10 June 2023).
34. Wei, X.; Sun, L.; Sun, Q.; Xu, S.; Zhou, H.; Du, C. Propagation velocity model of stress wave in longitudinal section of tree in different angular directions. *BioResources* **2019**, *14*, 8904–8922. [CrossRef]
35. Wei, X.; Du, C.; Xu, S.; Tian, C.; Yang, X.; Hu, L.; Pang, P. Research on stress wave wood nondestructive testing technology. *J. Phys. Conf. Ser.* **2022**, *2366*, 012035. [CrossRef]
36. Zhang, C.; Zhu, Z.; Wang, S.; Ren, X.; Shi, C. Stress wave propagation and incompatible deformation mechanisms in rock discontinuity interfaces in deep-buried tunnels. *Deep. Undergr. Sci. Eng.* **2022**, *1*, 25–39. [CrossRef]
37. Abou-Matar, H.; Goble, G.G. SPT dynamic analysis and measurements. *Geotech. Geoenviron. Eng.* **1997**, *123*, 921–928. [CrossRef]